Visual Neuroscience (2003), **20**, 511–521. Printed in the USA.

DOI: 10.1017/S0952523803205058

Chromatic detection and discrimination in the periphery: A postreceptoral loss of color sensitivity

JESSICA R. NEWTON AND RHEA T. ESKEW, JR.

Psychology Department, Northeastern University, 125 Nightingale Hall, Boston

(RECEIVED February 4, 2003; ACCEPTED August 5, 2003)

Abstract

The peripheral visual field is marked by a deterioration in color sensitivity, sometimes attributed to the random wiring of midget bipolar cells to cone photoreceptors in the peripheral retina (Mullen, 1991; Mullen & Kingdom, 1996). Using psychophysical methods, we explored differences in the sensitivity of peripheral color mechanisms with detection and discrimination of 2-deg spots at 18-deg eccentricity, and find evidence for a postreceptoral locus for the observed loss in sensitivity. As shown before, observers' sensitivity to green was lower than to red in the periphery, although the magnitude of this effect differed across observers. These results suggest that the asymmetry in peripheral sensitivity occurs at a postreceptoral site, possibly a cortical one. In addition, noise masking was used to determine the cone inputs to the peripheral color mechanisms. The masked detection contours indicate that the red and green mechanisms in the periphery respond to the linear difference of approximately equally weighted L- and M-cone contrasts, just as they do in the fovea. Thus, if the midget retinal ganglion system is responsible for red/green color perception in the fovea, it is likely to be responsible at 18-deg eccentricity as well.

Keywords: Color mechanisms, Chromatic detection, Chromatic discrimination, Periphery

Introduction

Like most other visual functions, color vision initiated by the long- (L) and middle- (M) wavelength-sensitive cone photoreceptors declines in the peripheral retina (Mullen, 1991; Stromeyer et al., 1992; Mullen & Kingdom, 1996). In particular, sensitivity to green decreases faster than to red with eccentricity. The present study explores the characteristics of peripheral color mechanisms, focusing on the green and red mechanisms, which receive input from the L and M cones, using detection and threshold-level discrimination procedures. We examine the asymmetric loss in sensitivity to green compared to red in the periphery as well as the cone inputs to these mechanisms, and the number of active mechanisms underlying detection of our stimuli.

One possible explanation for the observed selective loss in chromatic sensitivity with eccentricity, specifically the decrease in red–green sensitivity across the human visual field (Mullen, 1991; Stromeyer et al., 1992), is a change in the relative number of cones in the peripheral cone mosaic. Not only does overall cone density fall steeply with eccentricity, being one order of magnitude lower 1 mm out from the fovea (Curcio et al., 1990), the ratio of middle- to long-wavelength-sensitive cones (M to L cones) may also change. An mRNA analysis suggests that the M:L cone ratio in the central visual field is 2:3 and decreases to 1:3 by 40-deg eccentricity for most people (Hagstrom et al., 1998) (however, a more recent primate mRNA study by Deeb and his colleagues (2000) found no evidence for a change in the M:L cone ratio out to 45-deg eccentricity). An M:L cone ratio reduction would be particularly interesting in light of much psychophysical evidence indicating that sensitivity to "green" declines faster with eccentricity than sensitivity to "red." Studies of color appearance suggest that, at a fixed stimulus size, sensitivity to "green" declines faster in the periphery than sensitivity to "red" (Moreland & Cruz, 1959; Connors & Kelsey, 1961). When spot size is varied, "green" spots must be made larger than "red" ones to produce equivalent amounts of chromatic saturation (Abramov et al., 1991). This relative loss of "green" compared to "red" could be consistent with a lower M:L ratio in the periphery, because a lower proportion of M cones could lead to a relatively weaker "green" response to incremental lights. Incremental test lights (lights that are added to a background, which necessarily include a luminance component) were used exclusively in these older studies.

The convergence of multiple cones onto bipolar cells could also lead to a decline in red–green sensitivity in the periphery. The midget system, which is believed to mediate red and green detection in the fovea, has a lower density of ganglion cells in the periphery compared to the fovea (see Rodieck, 1998). There is a one-to-one connection between cones and ganglion cell centers *via* a midget bipolar cell in the fovea (Wässle & Boycott, 1991), whereas there is spatial convergence in the peripheral primate

Address correspondence and reprint requests to: Jessica R. Newton, MIT, Brain & Cognitive Sciences Department E25-235, 45 Carleton Street, Cambridge, MA 02139, USA. E-mail: jrnewton@mit.edu

retina (Wässle et al., 1994) beyond 7-deg eccentricity (Lee, 1996). The random organization of the M and L cones in monkey (Mollon & Bowmaker, 1992; Roorda et al., 2001) and human retinas (Roorda et al., 2001) suggests that there is unlabeled peripheral spatial convergence, decreasing overall red–green sensitivity by mixing the cone inputs to receptive-field centers. Spatial convergence in the midget system may be linked to peripheral sensitivity losses, with suprathreshold wavelength discrimination deteriorating between 25-deg and 40-deg in the middle- and long-wavelength regions, but only changing minimally from the fovea to 7-deg (Stabell & Stabell, 1984). Mullen and Kingdom (1996) find evidence consistent with random cone inputs for the decline in sensitivity to red–green grating patches.

However, a recent retinal physiological study suggests that the peripheral decline in red–green sensitivity may not be a retinal effect, but instead is produced at a higher visual stage (Martin et al., 2001). They found that P cells between 20- and 50-deg eccentricity were no less chromatically opponent than foveal P cells, despite being fed by many more cones. These cells may selectively sample L and M cones, maintaining chromatic opponency in the periphery. Therefore, Martin and colleagues (2001) argued that the decline in psychophysical chromatic sensitivity with eccentricity occurs outside the retina.

In the present study, we searched for additional evidence for a postreceptoral locus for the reduction in peripheral chromatic sensitivity. We measured detection contours in the $\Delta L/L$, $\Delta M/M$ plane of cone contrast space (see Eskew et al., 1999, for an introduction to this approach), concentrating on equiluminant and near-equiluminant tests for the following reason: Incremental green and red lights both produce +M and +L signals, of different relative magnitudes for green and red. In contrast, equiluminant green and red lights *equally* stimulate the L and M cones, but with opposite sign (Fig. 1A). The perception of "green" is elicited by both M-cone increments and L-cone decrements, whereas the perception of "red" is elicited by both L-cone increments and M-cone decrements (De Valois et al., 1997). Stromeyer et al. (1992) found a loss in sensitivity to equiluminant green compared to equiluminant red tests beyond 14-deg eccentricity, where both cone classes are stimulated identically (apart from sign) by both tests. Since cone responses to weak stimuli are linear (Schnapf et al., 1990), a green versus red loss that involves increments and decrements of equivalent magnitudes of L- and M-cone signals cannot be due to the cones themselves.

A closely related issue has to do with the slopes of the detection contours of the red and green detection mechanisms. In the $\Delta L/L$, $\Delta M/M$ plane of cone contrast space, *foveal* red and green psychophysical detection mechanisms are represented by long flanks that have approximately unit slope and cross the axes such that at threshold $-\Delta L/L \approx +\Delta M/M$, and $+\Delta L/L \approx -\Delta M/M$ (Fig. 1B). This unit slope implies that the L- and M-cone inputs to both detection mechanisms are equal in magnitude and opposite in sign (see Eskew et al., 1999, for review). In the periphery, Stromeyer et al. (1992) measured only a small number of thresholds that actually fell along unit-slope lines. They *assumed* linear, unit-slope red and green mechanisms, despite having only weak evidence for them beyond 14-deg eccentricity. The assumed unit-slope contours were extrapolated to both axes to support the authors' contention that peripheral sensitivity to $-\Delta L/L$ was approximately equal to $+\Delta M/M$ (both "green"), and sensitivity to $+\Delta L/L$ was approximately equal to $-\Delta M/M$ (both "red"). This is equivalent to assuming that the peripheral red and green mechanisms have the same relative cone weights as in the fovea. In addition, they did not conclusively identify the mechanisms underlying detection of their peripheral tests. The present study addresses these two issues, expanding upon the earlier findings by determining how many mechanisms are active at 18-deg eccentricity at threshold in the $\Delta L/L$, $\Delta M/M$ plane. The evidence for a postreceptoral locus for the peripheral red–green asymmetry is also examined, and the cone inputs to the peripheral green and red mechanisms are compared to the fovea.

Fitting our model to the detection thresholds amounts to making a hypothesis about the color mechanisms involved, as well as which mechanisms are responsible for detecting which stimuli under our particular conditions. To attempt to confirm that hypothesis, we used a discrimination procedure and a Bayesian classifier model, as we recently have done for foveal stimuli (Eskew et al., 2001). The logic of the discrimination procedure follows from Muller's law of specific nerve energy (Boring, 1942). Two "labeled line" assumptions (Watson & Robson, 1981; Graham, 1989) are made in this experiment. They are (1) that two stimuli that are

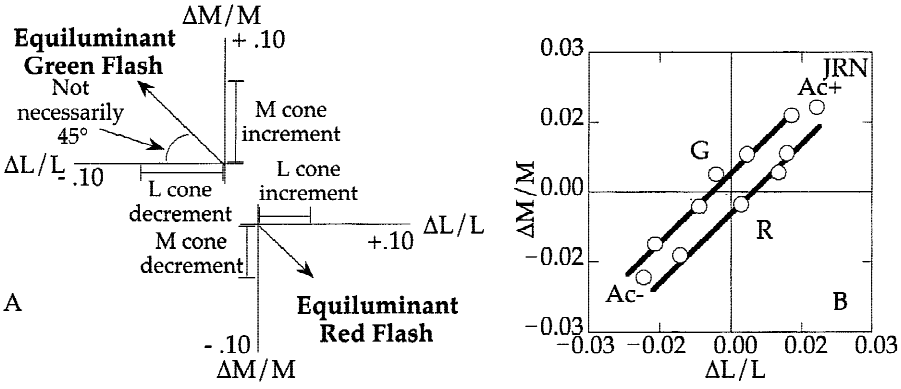

Fig. 1. (A) The ($\Delta L/L$, $\Delta M/M$) plane of cone contrast space with "exploded" axes. An approximately equiluminant, "green" threshold stimulus (upper vector) consists of both M-cone increments and L-cone decrements. The corresponding "red" threshold stimulus (lower vector) consists of both L-cone increments and M-cone decrements (of lower magnitudes). (B) Foveal detection contour for observer JRN in the $\Delta L/L$, $\Delta M/M$ plane. The open circles represent unmasked detection thresholds. Standard error bars are smaller than the symbols. The letters depict the approximate color appearance of nearby tests at threshold: green (G), red (R), increment achromatic (Ac+), or decrement achromatic (Ac−). The solid thick lines of unit slope represent hypothetical "green" and "red" detection mechanisms (see Eskew et al., 1999 for review). These data are represented in coordinates based on the Smith and Pokorny cone fundamentals.

Table 1. *Noise angles and noise contrasts*

Nominal noise direction	Observer	Actual ($\Delta L/L$, $\Delta M/M$, $\Delta S/S$)	Noise contrast	Actual angle (deg)
$(c,c,0)$	JRN	(0.20, 0.19, −0.01)	0.27	44
	JDA	(0.28, 0.27, −0.01)	0.38	44
(c,c,c)	JRN	(0.25, 0.25, 0.25)	0.43	45
	JDA	(0.25, 0.25, 0.25)	0.43	45

detected by a single chromatic mechanism can be made indistinguishable by adjusting their relative strengths, and (2) that two tests detected by two different chromatic mechanisms are as discriminable as they are detectable. By measuring the discriminability of pairs of threshold stimuli, we can test our detection model's assignment of regions of the detection contour to a particular color mechanism. Together, the detection and discrimination procedures allow a complete characterization of the mechanisms responsible for detection of our peripheral tests.

Materials and methods

Observers

Two well-practiced observers participated in these experiments. Both observers had normal color vision as assessed by the FM-100 test. Observer JRN is female and an author, and the other observer, JDA, is male. These experimental procedures were approved by the human subjects review committee of Northeastern University, in accordance with federal guidelines.

Apparatus

Test stimuli were generated on a Macintosh computer and displayed on a Nanao T560i monitor. The monitor was driven by a standard video card with 8-bit digital-to-analog converters (DACs). The steady background field produced by the monitor was circular (9.4-deg diameter), white ($x = 0.309, 0.331$), and 130 Td. This background field was continuously presented during all experiments.

Spectroradiometric calibration of the monitor was performed at 1.05-nm intervals over the spectrum. The monitor was linearized *via* gamma-correction lookup tables. A 2.4-mm-diameter artificial pupil was used. Chromatic aberration was minimized by means of a five-element achromatizing lens, which corrects for both lateral and longitudinal chromatic aberrations (Powell, 1981). Head position was stabilized with a dental-impression bite bar. A directly viewed grain-of-wheat bulb, placed off to the side in the dimly illuminated room, was used for peripheral fixation. The bulb was dimly illuminated at the minimum level that provided stable fixation.

Stimuli

Circular spots, 2 deg in diameter, were presented for 200 ms in the center of the background in either the fovea or at 18-deg eccentricity on the temporal retina. All stimuli are represented as vectors in the ($\Delta L/L$, $\Delta M/M$) plane of cone-contrast space (see Fig. 1A). The magnitude of the stimulus is specified by vector length in cone-contrast units (Stromeyer et al., 1985; Eskew et al., 1999).

In several experiments, the detection and discrimination tasks were performed in the presence of masking noise. Noise desensitizes mechanisms except for those with detection contours that are parallel to the noise direction (Giulianini & Eskew, 1998), and so noise directions parallel to the red and green detection contours were chosen. This noise masks mechanisms other than red and green, effectively exposing more of the red and green contours by making it more difficult for stimuli to be detected by other mechanisms.

The noise consisted of randomly flickering rings centered on and interdigitated with the test (see Giulianini & Eskew, 1998). The rings randomly and independently changed from one chromaticity to a symmetrically opposite chromaticity (on the opposite side of the white point, so that the mean chromaticity was unchanged). Each ring switched chromaticity with probability 0.5 at 16.8 Hz. The noise directions (polar angles in the plane) and strengths are given in Table 1. The noise contrast used was either the maximum possible, or the highest contrast that produced measurable masked thresholds in all color directions (judged on the basis of pilot experiments), in order to expose as much of the less sensitive mechanisms as possible.

Cone fundamentals

In the fovea, coordinates based on the Smith-Pokorny cone fundamentals were used (Smith & Pokorny, 1975). The 18-deg eccentric data, however, are represented in coordinates based on new peripheral cone fundamentals, calculated from the Stockman and Sharpe (2000) 10-deg fundamentals by altering the assumed macular pigment density to zero and assuming cone photopigment densities appropriate for 18-deg eccentricity: 0.21 (L, M) and 0.17 (S). No changes were made to the lens-density spectrum, which was obtained from Stockman and Sharpe (2000) and is a slightly modified version of the lens-density spectrum of van Norren and Vos (1974) (see Appendix for more details).

Color directions

The stimulus chromaticities were originally chosen based on the foveal cone fundamentals and an initial calculation of the peripheral cone fundamentals. After data collection, the data were reanalyzed for this paper using better estimates of the peripheral cone fundamentals, as described above. In a few instances this produced angles that were suboptimal in the new peripheral coordinates. The peripheral cone fundamentals resulted in a small S-cone modulation for our $\Delta L/L$, $\Delta M/M$ plane tests, ranging from 0.001 to 0.03 in cone-contrast units. The cone contrast produced by this modulation is well below the 0.07 no noise S-cone threshold obtained for 200 ms, 2-deg spots at 18-deg eccentricity for observer JRN.

Procedure

Detection thresholds were measured with a two-temporal-alternative forced choice (2AFC), adaptive-staircase method. The observer first adapted to the steady background for 90 s. He or she then initiated a run, consisting of 100 presentations of a single-test color direction of variable contrast. Each trial contained two 200-ms intervals, signaled by tones, separated by 400 ms. After each trial, the observer indicated in which interval the test was presented by pressing a button. Two independent staircases were randomly interwoven within a run. Test contrast was decreased by 0.1 log units after three consecutive correct responses and increased by the same amount after a single error. All of the frequency of seeing data for a given test chromaticity was accumulated and fit with a Weibull function to extract a threshold estimate (corresponding to 82% detection) and a psychometric slope estimate (Watson, 1979; Pelli & Zhang, 1991) for each run. Data figures show mean threshold and its standard error, based upon between-run variability. Two to four runs were obtained for most test conditions, with runs occurring in different sessions on different days.

In the discrimination experiments, two stimuli were fixed at their detection thresholds (82% 2AFC detection), and presented in the two intervals of a trial in random order. One color direction was designated as correct (the "standard"), and the observer learned from the feedback tones how to select the standard stimulus during practice runs. This discrimination procedure was previously described in more detail (Eskew et al., 2001).

Rod controls

The steady white background was 2.44 log scot Td, near rod saturation (Hood & Finkelstein, 1986). However, to be certain that rods did not directly detect our tests, we performed two types of rod controls. First, we performed a rod bleach, consisting of 1 min of 5.00 log scot Td of "white" light $[(x, y) = 0.38, 0.46]$. This light isomerizes about 80% of the rod photopigment (Hood & Finkelstein, 1986), enough to substantially raise rod thresholds. The bleaching field was 9.4 deg in diameter and centered on 18-deg eccentricity. After 1 min of bleaching, the field was extinguished and the observer waited 5 min in near darkness to reach the cone plateau. This was followed by 30 s of adaptation to the white monitor background, and 50 trials lasting less than 2.5 min. Equiluminant green and red test thresholds were measured at various spot sizes and durations, including those used in this study. Observer JRN showed no substantial effect of the bleach under any condition (unpublished data, not shown), and green thresholds were higher than red thresholds in both bleach and no-bleach conditions.

The second rod control was performed with a previously described procedure (McLellan & Eskew, 2000). A 4-log filter was used to attenuate the light from the monitor to −1.9 log scot Td. The observer adapted to this dim field for 20 min before performing 100 2AFC trials. The test was a 2-deg-diameter spot presented for 200 ms, as in the main experiment. Pooling over four runs in two different sessions, observer JRN was able to detect 0.555 ± 0.049 (95% binomial confidence limit) of a nominal M-cone increment spot (90 deg in the $\Delta L/L$, $\Delta M/M$ plane) when it was presented at the maximum available contrast. If rods obey Weber's law, they would detect these M-cone tests slightly better than chance under the brighter conditions of the main experiment. However, this was at maximum contrast, and the actual measured thresholds were usually below maximum contrast. Less formal measurements were made along the equiluminant red, green, and +S and −S cone as well as the achromatic directions, using a 0.125 cpd ($\sigma = 1$ deg), "raised Gabor" test (Tyler et al., 1992). Only the achromatic decrements were seen under these dim conditions (consistent with Patel & Jones, 1968) even at maximum contrast. We conclude that our test stimuli were not detected *via* rods.

Results

Detection results

The detection experiments in the $\Delta L/L$, $\Delta M/M$ plane of cone-contrast space at 18-deg eccentricity should reveal not only the magnitude of the asymmetry in sensitivity to green and red, but also whether or not this effect occurs at a postreceptoral site.

In the first experiment, the foveal detection contour in the $\Delta L/L$, $\Delta M/M$ plane of cone-contrast space was measured to provide a basis for comparison with respect to the sensitivity and cone inputs to the green and red mechanisms in the periphery. The circles in Fig. 1B represent the unmasked foveal detection thresholds in the $\Delta L/L$, $\Delta M/M$ plane of cone-contrast space, for one observer. Based upon informal reports from this observer, tests falling along the thick upper line appear green at threshold and those falling along the lower line appear red at threshold.

In the fovea, green and red mechanisms respond to the linear difference of equally weighted L- and M-cone contrast signals (Stromeyer et al., 1985; Cole et al., 1993; Chaparro et al., 1994). The lines indicate the loci of constant response for these two mechanisms (Eskew et al., 1999). For example, the equation of the upper line, representing the green mechanism, could be written

$$211\,\frac{\Delta M}{M} - 211\,\frac{\Delta L}{L} = 1. \qquad (1)$$

Both the green and red lines have approximately unit slope, indicating that both L and M cones provide inputs of equal magnitude to both mechanisms. The results of this experiment suggest that the L and M cones provide equal inputs to the green and red mechanisms, and that red and green foveal thresholds are equidistant from the origin, indicating that sensitivity to green and red is equal in the fovea.

In the second experiment, the peripheral detection contour in the $\Delta L/L$, $\Delta M/M$ plane of cone-contrast space was measured for the same observer as in Fig. 1 and an additional observer in order to investigate the changes in the sensitivity of the green and red mechanisms in the periphery. The circle symbols in Fig. 2A represent unmasked detection thresholds at 18-deg eccentricity, for the same observer as in Fig. 1B. The peripheral detection contour is dramatically different in shape from the foveal one, with the peripheral contour being more rounded and less elongated along the 45/225 deg direction. As several previous studies have shown, the red and green mechanisms are by far the most sensitive ones in the fovea (Chaparro et al., 1993), and their sensitivity decreases in the periphery (Stromeyer et al., 1992; Mullen & Kingdom, 1996). Thus, the shift in the overall shape of the detection contour in the periphery likely reflects the fact that the sensitivity of all the active mechanisms are more similar than in the fovea, and not dominated by the red and green mechanisms.

The threshold at 80 deg seemed inconsistent with the data from 45 deg to 90 deg, so this threshold was replicated in two separate experiments (upward and downward triangles), along with several

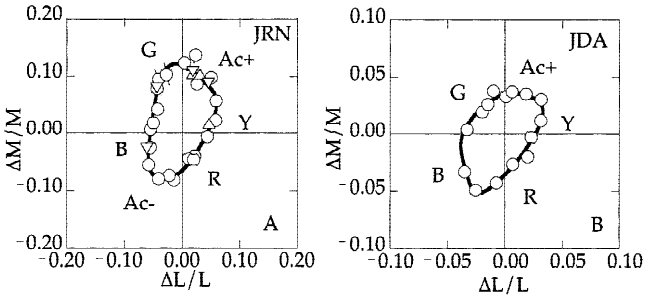

Fig. 2. 18-deg eccentric detection contours for observer JRN and JDA in the ($\Delta L/L$, $\Delta M/M$) plane (A & B, respectively). The circles show unmasked detection thresholds and the triangles show replications. Standard error bars are shown when the standard error is larger than the symbol. The letters depict the approximate color appearance of nearby tests at threshold: green (G), red (R), yellow (Y), blue (B), increment achromatic (Ac+), or decrement achromatic (Ac−). The line represents the smooth contour fit produced by the Minkowski combination of the six mechanism (or five for JDA) fit to the data. The circle at polar angle 80 deg in A was ignored in the smooth contour fit to the data. This test originally appeared green at threshold, but appeared as a white, transient blob on the two subsequent replications of the threshold at this angle (triangles). Thus this point was disregarded in the model fit because the threshold decreased substantially with practice, as shown in the position of the two replications. These data and those in subsequent figures are represented in coordinates based on the peripheral cone fundamentals.

other test directions for comparison. The results indicate that the threshold estimates are generally reliable, but that the first estimate at 80 deg had indeed been too high (see below and figure legend).

This observer informally described these peripheral spots using six color names; red, yellow, white (increment achromatic), green, blue, and dark (decrement achromatic). Fig. 2B shows analogous results for a second observer. This observer used only five color names to describe these stimuli; the decrement achromatic color was missing. The results of this experiment are consistent with previous work, and demonstrate that there is a greater loss in sensitivity to green compared to red at 18-deg eccentricity. Since this asymmetric sensitivity loss was observed with "green" stimuli consisting of both M-cone increments and L-cone decrements and the corresponding "red" stimuli consisting of both M-cone decrements and L-cone increments, the asymmetric thresholds indicate that the greater loss in green sensitivity occurs at a postreceptoral site and is not a cone level effect.

Detection model

The detection data were fit with smooth threshold contours. The mechanisms are assumed to be linear combinations of cone contrasts, with outputs that are stochastically independent and so are combined by probability summation. A tutorial introduction and review of this type of model is given elsewhere (see Eskew et al., 1999).

The informal color-appearance data was used as an initial guide in determining the number of mechanisms required to fit the data. For instance, in Fig. 2A, the observer used six color names and so six linear mechanisms were initially assumed for the model fit to this data (later we re-applied the model with fewer mechanisms, and found the fit to be worse; adding more than six mechanisms produced two mechanisms with essentially the same parameters). The model fit was produced when combinations of L- and M-cone contrasts were combined by a Minkowski summation rule (Quick, 1974; Graham, 1989):

$$\left(\sum_{i=1}^{6} |X_i|^{-C}\right)^{1/C} = 1. \qquad (2)$$

In this equation there are six mechanisms with responses X_i. The combination exponent, C, in this study is assumed to be 4.0. The size of this exponent controls the degree of rounding in the corners where two mechanisms have similar sensitivities (see Eskew et al., 1999), and values of C between about 2 and 4 are generally interpreted as representing probability summation among independent mechanisms (Graham, 1989). Each mechanism response is a weighted sum of cone contrasts, as in eqn. (1), that are here half-wave rectified such that the mechanism only responds to one polarity (i.e. red is a separate mechanism from green). For instance, the weighted sum for the red mechanism is given by

$$X_1 = R = U_R \rho_1 \left(W_{R,L} \frac{\Delta L}{L} + W_{R,M} \frac{\Delta M}{M} + W_{R,S} \frac{\Delta S}{S} \right). \qquad (3)$$

In this equation, U_R is the red-mechanism sensitivity, ρ is a half-wave rectification function, and the Ws represent relative cone-contrast weights. This is the same detection model that was used previously (Eskew et al., 2001), except that in the earlier study the pairs of mechanisms (e.g. red and green) were assumed to be fully symmetric: they had the same relative cone weights except they were of opposite sign (e.g. $W_{R,L} = -W_{G,L}$, $W_{R,M} = -W_{G,M}$, and $W_{R,S} = -W_{G,S}$), and the same sensitivities (e.g. $U_R = U_G$). Here, the yellow and blue, as well as the achromatic mechanisms were not assumed to be symmetric. For the red and green mechanisms, the relative cone weights were assumed to be symmetric, but the sensitivities were not. The standard model weights of Eskew et al. (1999) were used for the red and green mechanisms ($W_{R,L} = -W_{G,L} = 0.70$, $W_{R,M} = -W_{G,M} = -0.72$). This assumption constrains the red and green detected contours to essentially unit slope (0.70/0.72). Strong evidence for the assumed near-unit slope red and green mechanisms in the periphery is shown later in the masking noise experiments. The overall detection performance produced by the Minkowski combination of the six mechanisms is represented as the smooth detection contour in Fig. 2A.

Fig. 2B depicts the 18-deg eccentricity data for observer JDA. This observer used only five color names to describe the tests at threshold: red, yellow, white (achromatic increment), green, and blue. We attempted to fit a six-linear-mechanism model to this observer's data, but the sixth mechanism duplicated one of the other mechanisms in the fit. This suggests that only the five most sensitive mechanisms contribute to detection of the tests for this observer, consistent with the color names JDA used.

The Fig. 2A data are replotted in Fig. 3A with the solid lines now representing the threshold contour of each of the six linear mechanisms produced by the model fit (i.e. loci of constant X_i, without the Minkowski combination). Based upon the informal color names provided by the observer, we tentatively identify the mechanisms as (starting with the line closest to the "C" label and going clockwise) increment achromatic, yellow, red, decrement achromatic, blue, and green mechanisms. The green thresholds (near the upper unit slope line) are 2.1-fold further from the origin than the red thresholds (near the lower unit-slope line). The green-mechanism contour lies slightly outside the data points

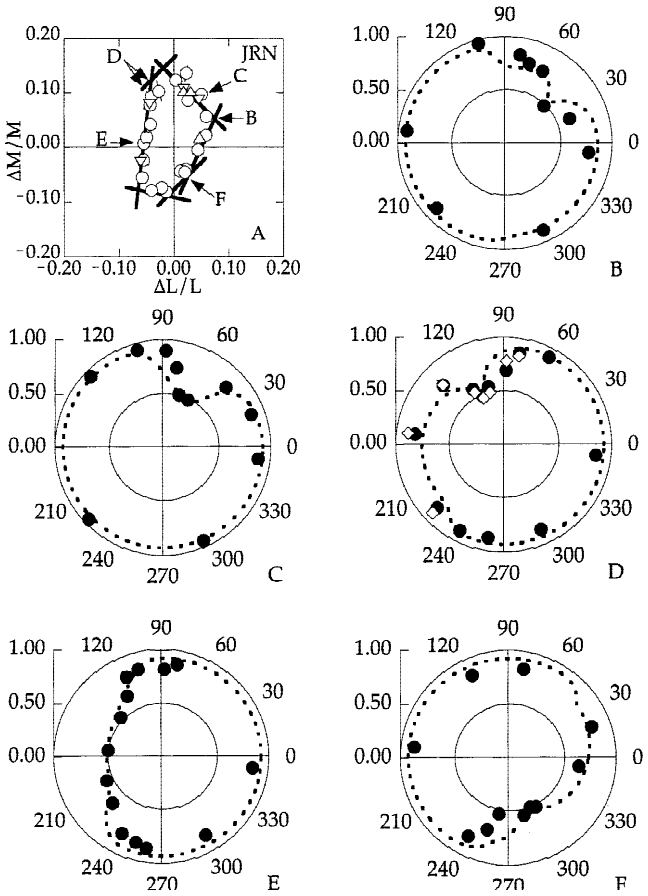

Fig. 3. (A) Same as Fig. 2A, except the threshold contours of the six mechanisms are shown rather than their Minkowski combination. Standard error bars are shown when the standard error is larger than the symbol. The arrows indicate the different stimuli used for standards in the discrimination experiment, with the letters referring to the panels showing the data for that standard. (B) Discrimination performance against the 44-deg standard, in polar coordinates. The angular coordinate represents the angle of the test (same angles as in A) and the distance of the filled circle from the origin represents the test's discriminability from the standard. The circumference of the inner circle corresponds to chance-level discrimination performance (50% discriminability), and the outer circle corresponds to perfect discrimination performance (100% discriminability). The dashed line is the prediction of the Bayesian classifier model based on the six-mechanism model fit to the detection data. Discrimination of the standard against itself was not actually measured. (C) Same as (b), but for the 63-deg standard. (D) Same as (b), but for the 105-deg (open diamonds) and the 113-deg standards (filled circles). The dashed line is the Bayesian classifier model fit for the 113-deg standard. (E) Same as (b), but for the 173-deg standard. (F) Same as (b), but for the 293-deg standard.

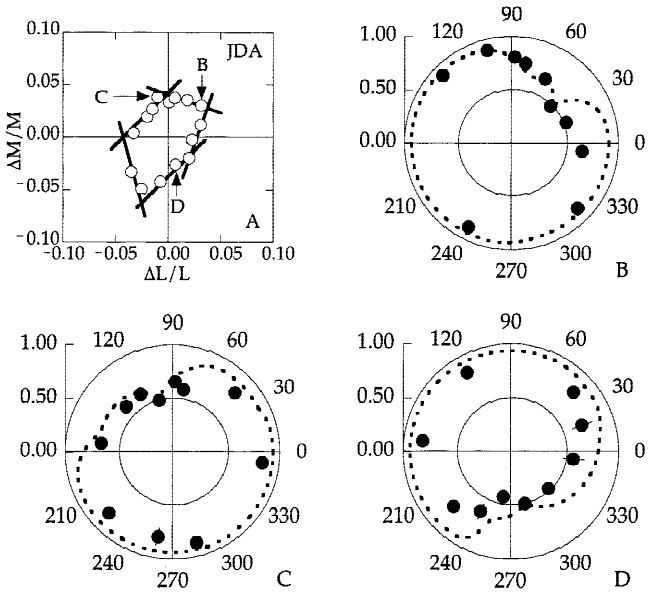

Fig. 4. (A) Same as Fig. 3, but for observer JDA. Standard error bars are shown when the standard error is larger than the symbol. (B) 44-deg standard. (C) 105-deg standard. (D) 285-deg standard.

because, in the region close to both the blue and Ac+ contours, the measured thresholds are reduced *via* probability summation among the three mechanisms with similar sensitivities. Note that the discrepant threshold at 80 deg, mentioned above, lies with the thresholds up to 105 deg parallel to the "green" detection contour, as if the observer were attending only to the "greenish" cue produced by the 80-deg test and ignoring the achromatic cue that would have produced a lower threshold. Indeed the observer felt that the appearance of this color angle was green on the original runs but achromatic on the replications.

The data from Fig. 2B are replotted in Fig. 4A. Again the solid lines represent threshold contours of the five linear mechanisms produced by the model fit to the data. The red and green thresholds for this observer are also asymmetric about the origin, with the green thresholds 1.4-fold further from the origin than the red thresholds.

Discrimination results

The discrimination procedure is used to confirm that the detection model has accurately identified the mechanisms contributing to threshold (Eskew et al., 2001). The arrows in Fig. 3A indicate the six standard stimuli used in the discrimination experiment. The standards are indicated in Fig. 3A by the letter identifying the panel that contains the data for this standard. For example, panel (b) represents discrimination against the 44-deg standard, labeled B in panel (a). In these polar plots, the angular coordinate represents the test-color direction [same angles as in panel (a)] and the distance of the symbol from the origin represents the test angle's discriminability from the standard. The circumference of the inner ring corresponds to chance-level performance (50% discrimination) and the outer ring corresponds to perfect performance (100% discrimination). For example, panel (b), which represents the 44-deg standard, shows that the test at 173 deg is nearly perfectly discriminable from the 44-deg standard (the point at 173 deg lies close to the outermost ring), but the test near 58 deg is imperfectly discriminable from this same standard. Two very similar standards (105 deg & 113 deg) were used in panel (d) because our initial analysis of the detection data suggested these might be detected by different mechanisms; the final analysis indicated that they both are detected by the probability sum of two mechanisms and thus it is not surprising that they produce very similar discrimination performance. The dashed lines are the Bayesian model predictions, described below.

The data show a region for each standard where discrimination is at chance, meaning that these test angles cannot be distinguished from the standard. These bands represent the different labeled line mechanisms. For instance, Fig. 3C shows that tests above 88 deg

and below 21 deg are well discriminated from the 63-deg standard, whereas the 73-deg test cannot be distinguished from this standard. Assuming the labeled line hypothesis, this chance-level discrimination implies that the 63- and 73-deg stimuli are detected by the same chromatic mechanism. Other labeled line mechanisms are identified in the remaining Fig. 3 panels. In Fig. 3D, discrimination performance against the 113-deg (filled circles) or 105-deg (open diamonds) standards results in a region of chance performance from 105 deg to 113 deg, whereas the 173-deg standard has a region of chance-level performance between 135 deg and 204 deg (Fig. 3E). Discrimination performance against the 293-deg standard yielded a region of 50% discrimination from 260 deg to 299 deg (Fig. 3F). The whole set of discrimination data, using standard assumptions about labeled lines, is consistent with the hypothesis that six mechanisms contribute to seeing these peripheral tests. Although we cannot rule out some of these six being "higher-order" color mechanisms (Krauskopf et al., 1986)—our experiments were primarily designed to isolate "red" and "green" mechanisms rather than exhaustively identify all the mechanisms—the simplest hypothesis is that these are the classical color mechanisms that correspond to the informal color names provided by the observer: red, green, yellow, blue, and increment and decrement achromatic (Eskew et al., 2001). Other test angles produced intermediate levels of discrimination, where performance was better than chance, but not perfect. For instance, the 119-deg test is imperfectly discriminated from both the 113-deg (Fig. 3D) and the 173-deg standard (Fig. 3E) (59% and 65%, respectively), and the 353-deg test is imperfectly discriminated from both the 44-deg (Fig. 3B) and the 293-deg standards (Fig. 3F) (78.5% and 65.5%, respectively). This intermediate discrimination performance can be explained by the probability summation of detection by two (or more) mechanisms. On a given trial, one mechanism, the other mechanism, or both mechanisms detect the test. On those trials in which both the test and standard are detected by the same mechanism, the observer cannot discriminate between the two. On other trials the test and standard will be detected by different mechanisms, and the observer will be able to discriminate between them. The net result is an intermediate level of performance.

Figs. 4B–4D show similar results for JDA. Due to the simpler shape of JDA's detection contour, it was possible to isolate the "red" and "green" mechanisms relatively easily, and only three standard colors were chosen. For the 44-deg standard (Fig. 4B), there is a region of near-chance performance between 21 deg and 44 deg. For the 285-deg standard (Fig. 4D), there is a spectral band from 261 deg to 315 deg. The 353-deg test is imperfectly discriminated from both the 44-deg standard (Fig. 4B) and the 285-deg standard (Fig. 4D) (66% and 58%, respectively), consistent with this stimulus being detected by the probability sum of two (or more) mechanisms. The results of this experiment suggest that these three standards are detected by three different labeled line mechanisms, consistent with the five-mechanism model. For each observer, the transition angles (where performance goes from chance-level to good) are in good agreement across standards. For example, Figs. 3B–3D all have a transition angle near 70–80 deg. A similar consistency in transition angle was found in the fovea where this consistency of transition angle across different standards for a given observer was interpreted as evidence for fixed color boundaries rather than discrimination based upon a distance in color space (Eskew et al., 2001). Although the two observer's detection models are quite different, they share some similar features—for example, tests from about 75 deg to 110 deg are detected by the probability sum of two mechanisms for both JRN and JDA. This results in a somewhat broad transition located near 70–80 deg for JDA as well (Figs. 4 & 4C).

Fixed color boundaries have been interpreted as evidence for categorical color perception, implying a limited number of color mechanisms (Wandell, 1985; Mullen & Kulikowski, 1990). Categorical perception occurs when stimuli that vary along a continuous physical dimension are given one label on one side of a category boundary and a different label on the other side of the boundary (Harnad, 1987). Here we expect category boundaries to correspond to the angles where the labeled line detection mecha-

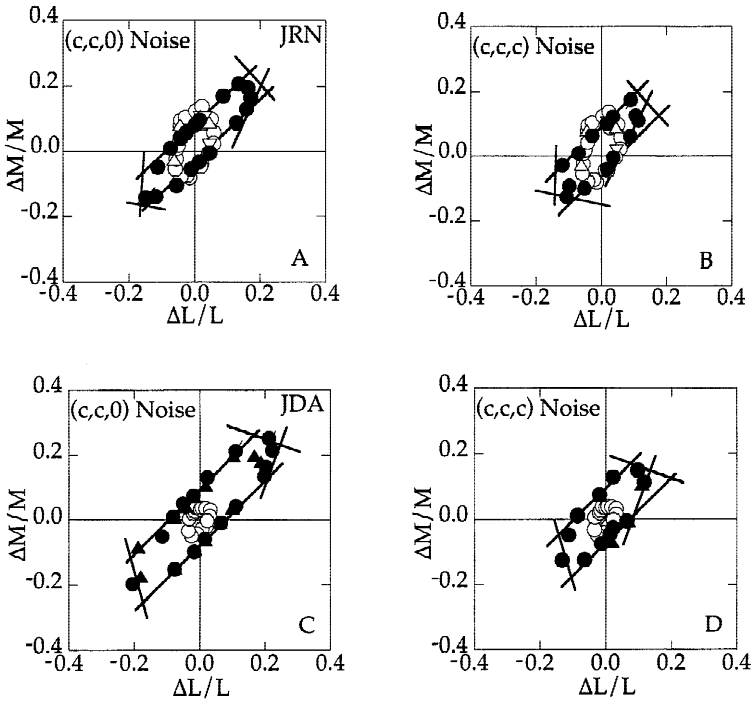

Fig. 5. Detection contours for observer JRN and JDA under two different noise-masking conditions. The open circles represent unmasked detection thresholds, replotted from Figs. 3A and 4A. The filled circles represent the masked thresholds and the filled triangles represent replications. Standard error bars are shown when the standard error is larger than the symbol. The solid lines show the detection mechanisms; these were constrained to have the same slopes (relative cone weights) estimated for the no-noise data. The noise levels used are shown in Table 1. The results for observer JRN under $(c,c,0)$ and (c,c,c) noise conditions are shown in panels A and B, respectively. The results for observer JDA in the $(c,c,0)$ and (c,c,c) noise conditions are shown in panels C and D, respectively.

nisms meet at the corners of the detection contours; the discrimination data are consistent with this expectation (see also Eskew et al., 2001).

Discrimination model

The dashed lines in panels (b)–(f) of Fig. 3 and panels (b)–(d) in Fig. 4 are the predictions of a Bayesian classifier model based upon the model fits to the detection data. The classifier computes the outputs of the six (five for JDA) detection mechanisms to both the test (I) and standard (II) and chooses the standard based upon the following rule: respond "I" if $P(\mathrm{I}|\Omega) \geq P(\mathrm{II}|\Omega)$, otherwise respond "II". $P(\mathrm{I}|\Omega)$ and $P(\mathrm{II}|\Omega)$ are the posterior probabilities of the stimuli presented given the set of Ω detection mechanism responses. When $P(\mathrm{I}) = P(\mathrm{II}) = 1/2$, then

$$P(\mathrm{I}|\Omega) = \frac{P(\Omega|\mathrm{I})}{P(\Omega|\mathrm{I}) + P(\Omega|\mathrm{II})}. \quad (4)$$

The functions $P(\Omega|\mathrm{I})$ and $P(\Omega|\mathrm{II})$ are "joint psychometric functions". For example, for JRN, $P(\Omega|\mathrm{I}) = P(\mathrm{r}|\mathrm{I})\,P(\mathrm{g}|\mathrm{I})\,P(\mathrm{b}|\mathrm{I})\,P(\mathrm{y}|\mathrm{I})\,P(\mathrm{Ac}-|\mathrm{I})\,P(\mathrm{Ac}+|\mathrm{I})$, the product of the likelihood that each of the six detection mechanisms (red, green, blue, yellow, decrement achromatic, and increment achromatic) detects the test (after correcting for guessing). These likelihoods are computed from the measured thresholds and an assumed psychometric slope of 4.0. These predictions are made with *no free parameters*. For more details about this model, see our previous paper (Eskew et al., 2001).*

Overall, in Fig. 3 the classifier did a good job of describing the discrimination performance. The model produced good predictions when discrimination performance was high, and reasonable predictions when it was near chance. In contrast, the model frequently overestimated discrimination performance in the transition region and for a few standards underpredicted performance in this region. The dashed lines in panels (b)–(d) of Fig. 4 are the predictions of the same Bayesian classifier model based upon a five-mechanism fit to JDA's detection data. The model does a good job of predicting performance for the 44-deg and 105-deg standards [panels (b) and (c)], but a poorer job for the 285-deg standard [panel (d)]. For this last standard, the chance performance region is larger than predicted, and the prediction in the transition regions exceeds actual performance.

There are several possible sources for the discrepancies between the classifier's predictions and the observer's performance. The mechanism weights and sensitivities in the detection model may be in error, or the observer may not optimally combine the information from the mechanisms. The correction for guessing used to generate the joint psychometric function, which is only approximately correct (see Eskew et al., 2001), may cause discrepancies. Finally, the assumed psychometric slope may be incorrect, although altering this slope has a relatively small effect on the predictions as a rule. Given that no free parameters are used in the classifier, we feel the model comes remarkably close to the measured discrimination.

An alternate explanation of the discrimination performance is that it is determined solely by Euclidean distance from the standard and is independent of labeled line mechanisms. However, when discriminability is plotted versus Euclidean distance in cone-contrast units (not shown), the data do not support this argument: for example, the distance in cone-contrast space corresponding to 82% discrimination performance varies from 0.052 to 0.097 across discrimination standards for observer JRN.

Noise masking detection results

The noise-masking experiments should reveal the cone inputs to the green and red mechanisms by desensitizing other mechanisms. In the fovea, the green and red mechanisms have nearly-equal and opposite cone weights, producing unit-slope detection contours in the $\Delta L/L$, $\Delta M/M$ plane of cone-contrast space (Cole et al., 1993; Chaparro et al., 1994; Chaparro et al., 1995; Sankeralli & Mullen, 1996; Sankeralli & Mullen, 1997). Stromeyer et al. (1992) *assumed* that the peripheral red and green mechanisms had unit slopes. In Figs. 3A and 4A, we constrained our model fits to have two mechanisms with unit slopes. In the current experiments, we used masking noises to expose more of the putative green and red mechanisms, to test our unit-slope assumption and to see if the peripheral red and green mechanisms are indeed like those found in the fovea.

The noise consisted of randomly flickering rings centered on the test spot (see Methods). Two different noise chromaticities were used: $(\Delta L/L, \Delta M/M, \Delta S/S) = (c, c, 0)$, *and* (c, c, c) (achromatic noise), where c is *a* constant contrast. These chromaticities were calculated using our preliminary cone fundamentals (see Methods). When plotted in our final, peripheral color space the actual angle of the $(c, c, 0)$ noise differs slightly from our original intention. The $(c, c, 0)$ noise, which appears "yellow" and "blue," corresponds to an angle of 44 deg in the $\Delta L/L$, $\Delta M/M$ plane of cone-contrast space, rather than the intended 45 deg. This noise was chosen because it should not affect unit-slope mechanisms (even with the 1-deg discrepancy), but masks other active detection mechanisms. The achromatic (c, c, c) noise was chosen to ensure that the nominal red and green tests were detected by chromatic and not luminance mechanisms. This achromatic noise, which appears "white" and "black," has a cone-contrast vector that extends out of the $\Delta L/L$, $\Delta M/M$ plane because it also includes S-cone modulation, but projects onto the 45-deg direction.

In Fig. 5, detection results in the presence of two different noise masks are shown for the two observers. The color angles to be tested were chosen on the basis of pilot data to efficiently sample the masked detection contour, and therefore not all the angles were the same as those tested without noise. The filled circles represent the masked detection thresholds and the open symbols represent the unmasked detection thresholds. Although the red–symmetry is still apparent in both noise conditions for both observers, there were mechanism fitted changes in the measured thresholds. The lines show the masked data. For each observer, we constrained the *relative* L-to-M cone weights for all six (JRN) and five (JDA) detection mechanisms to be the same as those fitted to the no-noise data (Figs. 3A & 4A). We allowed the sensitivity of these mechanisms to vary freely in the fits. Thus, the lines drawn in Fig. 5 have the same slopes as the lines in Figs. 3A and 4A, but are of different distances from the origin, showing facilitation or masking compared to the no-noise condition.

*One difference between the present application of this model and the Eskew et al.'s paper (2001) has to do with the stimulus contrasts we selected as the inputs to the classifier. In our previous paper, we used the contrasts of the detection tests as our inputs to the classifier, and so could only make predictions at the angles actually measured in the detection contours. In the present work, we used the model fits to the data (the smooth lines in Fig. 2) to define these inputs. This issue is discussed in the Appendix to Eskew et al. (2001). The two procedures produced similar predictions in this study, but the model-based predictions we used allowed us to compute the discrimination performance at every angle, not just the angles studied in the detection task.

Table 2. *Noise masking and facilitation*

Nominal noise direction	Mechanism	JRN Sensitivity factor	JDA Sensitivity factor
$(c,c,0)$	Green	2.04	0.44
	Red	1.51	0.49
	Achromatic +	0.32	0.13
	Achromatic −	0.46	—
	Yellow	0.42	0.18
	Blue	0.39	0.18
(c,c,c)	Green	1.79	0.44
	Red	1.39	0.54
	Achromatic +	0.42	0.21
	Achromatic −	0.62	—
	Yellow	0.73	0.36
	Blue	0.46	0.27

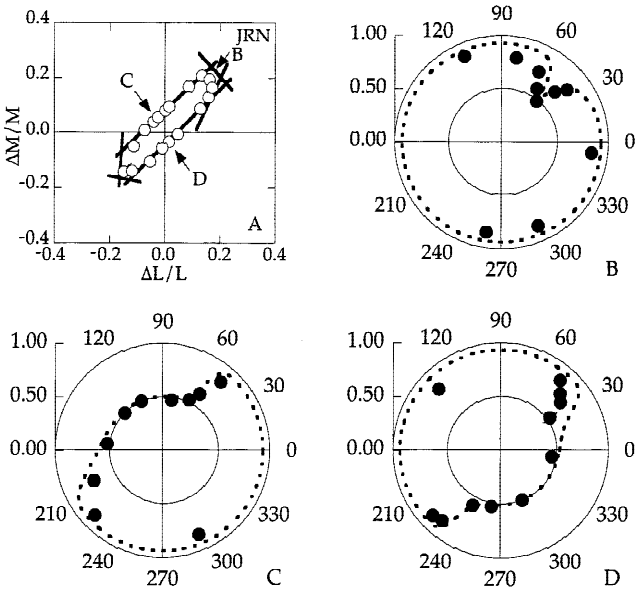

Fig. 6. (A) Masked detection contour for observer JRN in the $(c,c,0)$ noise condition. Data and model are identical to Fig. 5A. (B) Discrimination performance against the 50-deg standard, in the presence of masking noise, with the same format as in Figs. 3 and 4. (C) 113-deg standard. (D) 293-deg standard.

The change in sensitivity of the various mechanisms under different noise-masking conditions is shown in Table 2. For example, in the first line of the table the sensitivity factor for the green mechanism is 2.04, meaning that the weights of the mechanism have doubled in the $(c,c,0)$ noise-masking condition (or the mechanism thresholds decreased by half). In Fig. 5A, as in the no-noise case, the green thresholds are further from the origin than the red thresholds. For observer JRN, however, there is facilitation in green and red mechanisms in the presence of $(c,c,0)$ noise compared to the no-noise condition. Similar facilitation of the green and red mechanisms was observed in the (c,c,c) noise-masking case (Fig. 5B) for observer JRN. Giulianini and Eskew (1998) also found facilitation of detection in the presence of ring masking noise. They showed that the ring noise facilitated detection by reducing uncertainty in the spatial location of the test, since the concentric noise rings indicate the test location. The results for observer JDA also had the red–green asymmetry maintained in both noise-masking conditions, but differed from observer JRN in that both green and red mechanisms were masked in both noise conditions (see Table 2).

For both observers, in both cases, the two unit-slope lines fit the red and green thresholds well. This provides strong evidence that red and green have approximately equal magnitude for the L- and M-cone contrast weights in the periphery, just as they do in the fovea.

Masked discrimination

A discrimination experiment was performed in the presence of masking noise to further confirm that the unit-slope lines represent isolated labeled line detection mechanisms. Discrimination performance was measured in the presence of $(c,c,0)$ noise for JRN and is represented as in Fig. 3. Panel (a) in Fig. 6 shows the $(c,c,0)$ detection thresholds used in the discrimination procedure. The lines represent the six-mechanism fit to the detection data, as in Fig. 5A. The discrimination data is shown in panels (b)–(d), with the dashed line representing new Bayesian classifier model predictions, now based upon the detection model for the masked data (Fig. 5A). As before, these data show a region for each standard where discrimination is at chance, meaning that these tests cannot be distinguished from the standard. However, the flank corresponding to the green mechanism was expanded, with tests from 63 deg to 173 deg being poorly discriminated from the 113-deg standard [panel (c)]. A comparison of these results with Fig. 3D shows that the $(c,c,0)$ noise has masked other mechanisms, allowing the green mechanism to detect a wider range of tests. The band corresponding to the red mechanism was also expanded, with tests from 243 deg to 34 deg indistinguishable from the 293-deg standard [panel (d)] in the presence of $(c,c,0)$ noise.

As in the no-noise experiment, these data also show tests with intermediate discrimination. The 57-deg test is imperfectly discriminated from either the 50-deg standard [panel (b)] or the 113-deg standard [panel (c)] (59.5% and 63%, respectively), consistent with this stimulus being detected by the probability sum of multiple mechanisms. The 39-deg test is imperfectly discriminated from either the 50-deg standard [panel (b)] or the 293-deg standard [panel (d)] (78% and 71%, respectively). The consistency of transition angles across different standards is again suggestive of categorical color boundaries, which can be altered by masking of the underlying mechanisms.

As before, the model predictions do a good job of predicting discrimination performance, especially given that there are no free parameters. The model tends to predict better performance in the transition region than was obtained experimentally, as it does in the no-noise condition (for discussion see Eskew et al., 2001).

General discussion

These results suggest that six or five rectified linear mechanisms, for different observers, are necessary and sufficient to account for no-noise detection at 18-deg eccentricity. The discrimination results also suggest that there is categorical color perception, with evidence for fixed color boundaries. These same mechanisms, treated as labeled lines and used as the basis for a Bayesian classifier, also account for the discrimination performance. In addition, two different noise chromaticities were used to elevate

thresholds, thereby revealing more of the green and red mechanisms in the periphery. These mechanisms have approximately equal and opposite L- and M-cone inputs, implying near-unit slope, as has been repeatedly found in the fovea (Stromeyer et al., 1985; Cole et al., 1993; Chaparro et al., 1994) and assumed in the periphery by Stromeyer et al. (1992). The number of mechanisms found in this study are comparable to the number of classical mechanisms reported in central vision (Eskew et al., 2001).

Green sensitivity is lower than red sensitivity in the periphery, as has been shown before (Stromeyer et al., 1992). For JRN this asymmetry was a factor of 2, whereas for JDA the asymmetry was a factor of 1.4. Although these asymmetries are not large, they are substantial enough to make easily observed differences in sensitivity to small targets, and available evidence suggests the asymmetry is still larger further out in the periphery (Abramov et al., 1991; Stromeyer et al., 1992). In terms of relating psychophysics to physiology, experiments that use bipolar, red, and green stimuli inevitably underestimate the decline in sensitivity to "green." Examples include Martin et al. (2001), who used red/green flicker in their electrophysiological and psychophysical experiments, and Mullen and Kingdom (1996), who used red/green equiluminant gratings. If sensitivity to red is much greater at a given eccentricity, then the red mechanism will dominate the red/green sensitivity measurements and the overall chromatic loss will be underestimated.

The unit-slope red and green mechanisms demonstrated here are consistent with the foveal and peripheral color mechanisms being served by the same anatomical system. However the midget system, which is believed to underlie red–green detection in the fovea, undergoes spatial convergence in the midperiphery and becomes nonopponent in the far periphery (Dacey, 1999). Thus, the midget system clearly cannot underlie red–green detection in the far periphery. Our results suggest that if the midget system provides the basis for foveal red and green vision, it also does so at 18-deg eccentricity.

Our results, like those of Stromeyer et al. (1992), show that sensitivity to approximately equiluminant red and green tests is unequal in the periphery. By clearly showing that detection of these tests is served by a linear mechanism of unchanging unit slope, we have confirmed that the loss of sensitivity to "green" involves both $-\Delta L/L$ and $+\Delta M/M$ signals. A red–green asymmetry that involves both $-\Delta L/L$ and $+\Delta M/M$ is inconsistent with a retinal level effect, because such a difference should be reflected in a decrease in the number or gain of both L-cone OFF and M-cone ON center cells compared to both L-cone ON and M-cone OFF center cells. No such differences have been reported at the retinal level. The same is true for lateral geniculate nucleus (LGN) cells, where no differences between L- and M-cone ON and OFF center cells, consistent with our results, have been reported. Therefore, it seems likely that the observed red–green sensitivity difference arises at the cortical level. Double-opponent cells have been reported to exist in V1 (Hubel & Wiesel, 1968; Gouras, 1974; Michael, 1978; Livingstone & Hubel, 1984; Tootell et al., 1988) and secondary visual area V2 (Kiper et al., 1997). Double opponent cells represent a correlation between L-cone ON and M-cone OFF (and M-cone ON and L-cone OFF) pathways and thus would seem to offer a more likely locus for the observed red–green asymmetry.

Acknowledgments

This research was supported by NIH grant EY09712. We thank Jim Akula for his diligent efforts as an observer and Andrew Stockman for his suggests on cone fundamentals, as well as John Coley and Adam Reeves for comments on a draft of the manuscript.

References

Abramov, I., Gordon, J. & Chan, H. (1991). Color appearance in the peripheral retina: Effects of stimulus size. *Journal of the Optical Society of America A* **8**, 404–414.

Bone, R.A., Landrum, J.T., Fernandez, L. & Tarsis, S.L. (1988). Analysis of the macular pigment by HPLC: Retinal distribution and age study. *Investigative Ophthalmology and Visual Science* **29**, 843–849.

Boring, E.G. (1942). *Sensation and Perception in the History of Experimental Psychology*. New York: Appleton-Century-Crofts, Inc.

Bowmaker, J.K. & Dartnall, H.J. (1980). Visual pigments of rods and cones in a human retina. *Journal of Physiology* **298**, 501–511.

Chaparro, A., Stromeyer, C.F., III., Huang, E.P., Kronauer, R.E. & Eskew, R.T., Jr. (1993). Colour is what the eye sees best. *Nature* **361**, 348–350.

Chaparro, A., Stromeyer, C.F., III, Kronauer, R.E. & Eskew, R.T., Jr. (1994). Separable red–green and luminance detectors for small flashes. *Vision Research* **34**, 751–762.

Chaparro, A., Stromeyer, C.F., III, Chen, G. & Kronauer, R.E. (1995). Human cones appear to adapt at low light levels: Measurements on the red–green detection mechanism. *Vision Research* **35**, 3103–3118.

Cole, G.R., Hine, T. & McIlhagga, W. (1993). Detection mechanisms in L-, M-, and S-cone contrast space. *Journal of the Optical Society of America A* **10**, 38–51.

Connors, M.M. & Kelsey, P.A. (1961). Shape of the red and green color zone gradients. *Journal of the Optical Society of America* **51**, 874–877.

Curcio, C.A., Sloan, K.R., Kalina, R.E. & Hendrikson, A.E. (1990). Human photoreceptor topography. *Journal of Comparative Neurology* **292**, 497–523.

Dacey, D.M. (1999). Primate retina: Cell types, circuits and color opponency. *Progress in Retinal and Eye Research* **18**, 737–763.

Deeb, S.S., Diller, L.C., Williams, D.R. & Dacey, D.M. (2000). Interindividual and topographical variation of L:M cone ratios in monkey retinas. *Journal of the Optical Society of America A* **17**, 538–544.

De Valois, R.L., De Valois, K.K., Switkes, E. & Mahon, L. (1997). Hue scaling of isoluminant and cone-specific lights. *Vision Research* **37**, 885–897.

Eskew, R.T., Jr., McLellan, J.S. & Giulianini, F. (1999). Chromatic detection and discrimination. In *Color Vision: From Genes to Perception*, ed. Gegenfurtner, K. & Sharpe, L.T., pp. 345–368. Cambridge, United Kingdom: Cambridge University Press.

Eskew, R.T., Jr., Newton, J.R. & Giulianini, F. (2001). Chromatic detection and discrimination analyzed by a Bayesian classifier. *Vision Research* **41**, 893–909.

Giulianini, F. & Eskew, R.T., Jr. (1998). Chromatic masking in the (ΔL/L, ΔM/M) plane of cone-contrast space reveals only two detection mechanisms. *Vision Research* **38**, 3913–3926.

Gouras, P. (1974). Opponent-colour cells in different layers of foveal striate cortex. *Journal of Physiology* **238**, 583–602.

Graham, N.V.S. (1989). *Visual Pattern Analyzers*. New York: Oxford University Press.

Hagstrom, S.A., Neitz, J & Neitz, M. (1998). Variations in cone populations for red–green color vision examined by analysis of mRNA. *Neuroreport* **9**, 1963–1967.

Harnad, S. (1987). Introduction: Psychophysical and cognitive aspects of categorial perception: A critical review. *Categorical Perception*. Cambridge, United Kingdom: Cambridge University Press.

Hendrickson, A. & Drucker, D. (1992). The development of parafoveal and mid-peripheral human retina. *Behavioural Brain Research* **49**, 21–31.

Hood, D.C. & Finkelstein, M.A. (1986). Sensitivity to light. In *Handbook of Perception and Human Performance. Volume 1: Sensory Processes and Perception*, ed. Boff, K.R., Kaufman, L. & Thomas, J.P., pp. 5-1–5–66. New York: Wiley.

Hubel, D.H. & Wiesel, T.N. (1968). Receptive fields and functional architecture of monkey striate cortex. *Journal of Physiology* **195**, 215–243.

Kiper, D.C., Fenstemaker, S.B. & Gegenfurtner, K.R. (1997). Chromatic properties of neurons in macaque area V2. *Visual Neuroscience* **14**, 1061–1072.

Krauskopf, J., Williams, D.R., Mandler, M.B. & Brown, A.M. (1986). Higher order color mechanisms. *Vision Research* **26**, 23–32.

Lee, B.B. (1996). Receptive field structure in the primate retina. *Vision Research* **36**, 631–644.

Livingstone, M.S. & Hubel, D.H. (1984). Anatomy and physiology of a color system in the primate visual cortex. *Journal of Neuroscience* **4**, 309–356.

MARTIN, P.R., LEE, B.B., WHITE, A.J.R., SOLOMON, S.G. & RUTTIGER, L. (2001). Chromatic sensitivity of ganglion cells in the peripheral primate retina. *Nature* **410**, 933–936.
MCLELLAN, J.S. & ESKEW, R.T., JR. (2000). ON and OFF S-cone pathways have different long-wave cone inputs. *Vision Research* **40**, 2449–2465.
MICHAEL, C.R. (1978). Color vision mechanisms in monkey striate cortex: Dual-opponent cells with concentric receptive fields. *Journal of Neurophysiology* **41**, 572–588.
MOLLON, J.D. & BOWMAKER, J.K. (1992). The spatial arrangement of cones in the primate fovea. *Nature* **360**, 677–679.
MORELAND, J.D. & CRUZ, A. (1959). Colour perception with the peripheral retina. *Optica Acta* **6**, 117–151.
MULLEN, K.T. (1991). Colour vision as a post-receptoral specialization of the central visual field. *Vision Research* **31**, 119–130.
MULLEN, K.T. & KULIKOWSKI, J.J. (1990). Wavelength discrimination at detection threshold. *Journal of the Optical Society of America A* **7**, 733–742.
MULLEN, K.T. & KINGDOM, F.A. (1996). Losses in peripheral colour sensitivity predicted from "hit and miss" post-receptoral cone connections. *Vision Research* **36**, 1995–2000.
PATEL, A.S. & JONES, R.W. (1968). Increment and decrement visual thresholds. *Journal of the Optical Society of America* **58**, 696–699.
PELLI, D.G. & ZHANG, L. (1991). Accurate control of contrast on microcomputer displays. *Vision Research* **31**, 1337–1350.
POLYAK, S.L. (1941). *The Retina*. Chicago, Illinois: University of Chicago Press.
POWELL, I. (1981). Lenses for correcting chromatic aberration of the eye. *Applied Optics* **20**, 4152–4155.
QUICK, R.F., JR. (1974). A vector-magnitude model of contrast detection. *Kybernetik* **16**, 65–67.
RODIECK, R.W. (1998). *The First Steps in Seeing*. Sunderland, Massachusetts: Sinauer.
ROORDA, A., METHA, A.B., LENNIE, P. & WILLIAMS, D.R. (2001). Packing arrangement of the three cone classes in primate retina. *Vision Research* **41**, 1291–1306.
SANKERALLI, M.J. & MULLEN, K.T. (1996). Estimation of the L-, M-, and S-cone weights of the postreceptoral detection mechanisms. *Journal of the Optical Society of America A* **13**, 906–915.
SANKERALLI, M.J. & MULLEN, K.T. (1997). Postreceptoral chromatic detection mechanisms revealed by noise masking in three-dimensional cone contrast space. *Journal of the Optical Society of America A* **14**, 2633–2646.
SCHNAPF, J.L., NUNN, B.J., MEISTER, M. & BAYLOR, D.A. (1990). Visual transduction in cones of the monkey Macaca fascicularis. *Journal of Physiology* **427**, 681–713.
SHARPE, L.T. & STOCKMAN, A. (1999). Rod pathways: The importance of seeing nothing. *Trends in Neurosciences* **22**, 497–504.
SHARPE, L.T., STOCKMAN, A., KNAU, H. & JAGLE, H. (1998). Macular pigment densities derived from central and peripheral spectral sensitivity differences. *Vision Research* **38**, 3233–3239.
SMITH, V.C. & POKORNY, J. (1975). Spectral sensitivity of the foveal cone photopigments between 400 and 500 nm. *Vision Research* **15**, 161–171.
STABELL, U. & STABELL, B. (1984). Color-vision mechanisms of the extrafoveal retina. *Vision Research* **24**, 1969–1975.
STOCKMAN, A. & SHARPE, L.T. (2000). The spectral sensitivities of the middle- and long-wavelength-sensitive cones derived from measurements in observers of known genotype. *Vision Research* **40**, 1711–1737.
STOCKMAN, A., SHARPE, L.T. & FACH, C. (1999). The spectral sensitivity of the human short-wavelength sensitive cones derived from thresholds and color matches. *Vision Research* **39**, 2901–2927.
STROMEYER, C.F., III, COLE, G.R. & KRONAUER, R.E. (1985). Second-site adaptation in the red–green chromatic pathways. *Vision Research* **25**, 219–237.
STROMEYER, C.F., III., LEE, J. & ESKEW, R.T., JR. (1992). Peripheral chromatic sensitivity for flashes: A post-receptoral red–green asymmetry. *Vision Research* **32**, 1865–1873.
TOOTELL, R.B., SILVERMAN, M.S., HAMILTON, S.L., DE VALOIS, R.L. & SWITKES, E. (1988). Functional anatomy of macaque striate cortex. III. Color. *Journal of Neuroscience* **8**, 1569–1593.
TYLER, C.W., CHAN, H. & LIU, L. (1992). Different spatial tunings for ON and OFF pathway stimulation. *Ophthalmic and Physiological Optics* **12**, 233–240.
VAN NORREN, D. & VOS, J.J. (1974). Spectral transmission of the human ocular media. *Vision Research* **14**, 1237–1244.
WANDELL, B.A. (1985). Color measurement and discrimination. *Journal of the Optical Society of America A* **2**, 62–71.
WÄSSLE, H. & BOYCOTT, B.B. (1991). Functional architecture of the mammalian retina. *Physiological Reviews* **71**, 447–480.
WÄSSLE, H., GRUNERT, U., MARTIN, P.R. & BOYCOTT, B.B. (1994). Immunocytochemical characterization and spatial distribution of midget bipolar cells in the macaque monkey retina. *Vision Research* **34**, 561–579.
WATSON, A.B. (1979). Probability summation over time. *Vision Research* **19**, 515–522.
WATSON, A.B. & ROBSON, J.G. (1981). Discrimination at threshold: Labelled detectors in human vision. *Vision Research* **21**, 1115–1122.

Appendix—Cone fundamentals

In this paper, the data are represented in peripheral cone fundamentals based on the 10-deg fundamentals of Stockman and Sharpe (2000) with a peak macular pigment density of zero and peak photopigment optical densities of 0.21, 0.21, and 0.17 for the L, M, and S cones, respectively. We assumed a macular pigment density of zero beyond 10-deg eccentricity (Bone et al., 1988). According to Stockman and Sharpe (2000), mean peak photopigment optical densities of 0.50, 0.50, and 0.40 for the L-, M-, and S-cone fundamentals, respectively, are appropriate for the central fovea. The photopigment optical densities used in our peripheral cone fundamentals are lower than in the fovea because optical density decreases with eccentricity. A foveal cone outer segment length of 35 μm (Polyak, 1941) produces an axial peak photopigment optical density of approximately 0.5 (Bowmaker & Dartnall, 1980). Near 18-deg eccentricity the L- and M-cone outer segments are between 15 μm to 23 μm (Hendrickson & Drucker, 1992; Sharpe et al., 1998). As for S cones, in the periphery (greater than 5 mm or $>$ 18-deg eccentricity) their outer segments are thought to be 15–20% shorter than the outer segments of L and M cones (Sharpe & Stockman, 1999). To estimate peripheral peak optical densities, we scaled the foveal densities by the ratio of the peripheral-to-foveal outer segment lengths, yielding densities of 0.21, 0.21, and 0.17 for the L, M, and S cones, respectively. Stockman and colleagues (1999) estimated changes in S-cone photopigment optical density by measuring spectral sensitivity in the fovea and at 13-deg eccentricity and found mean changes in S-cone optical photopigment density, for five color normal observers, of 0.23. If a foveal S-cone optical density of 0.4 is assumed, these results suggest a peripheral peak optical density for the S cones of 0.17 at 13-deg eccentricity, the same value we used at 18-deg eccentricity.

The 18-deg eccentricity detection results presented in this paper were reanalyzed using the Smith–Pokorny (1975) foveal cone fundamentals for comparison with our peripheral cone coordinates (data not shown). The overall shape of the detection contours was slightly altered when using the foveal cone fundamentals, especially for JRN who had the higher thresholds. However, the main conclusions of the detection experiment were unchanged: six (JRN) or five (JDA) linear mechanisms accounted for the detection and discrimination data well, and the slopes of the mechanism contours were very little changed from those in the space defined by the peripheral cone fundamentals. In particular, unit-slope red and green mechanisms still fit those portions of the data quite well.

For observer JRN, the 18-deg eccentricity discrimination results were also reanalyzed using the foveal cone coordinates (data not shown). The discrimination predictions, based upon the adjusted cone coordinate detection data, still fit the discrimination data well. Thus, for both the detection and discrimination experiments, our overall conclusions hold across a range of different cone coordinate choices.